J Mater Sci (2006) 41:5099–5107
DOI 10.1007/s10853-006-0437-5

Au–Sapphire (0001) solid–solid interfacial energy

Hila Sadan · Wayne D. Kaplan

Received: 19 September 2005 / Accepted: 30 December 2005 / Published online: 27 July 2006

Abstract This work presents an experimental methodology for the measurement of interfacial energy (γ_{SP}) and work of adhesion (W_{ad}) of a metal–ceramic interface. A thin Au film was dewetted on the basal surface of sapphire substrates to form submicron-sized particles, which were analyzed using the Winterbottom method to determine the equilibrated particle–substrate solid–solid interfacial energy. Electron microscopy showed that a large portion of the particles contained grain boundaries, while all of the single crystalline particles had three distinct morphologies and orientations with the substrate. Two orientation relationships were determined from transmission electron microscopy, for which the interfacial energy in air at 1000 °C was determined: Au (111)–sapphire (0001): $\gamma_{SP} = 2.15 \pm 0.04$ J/m^2, $W_{ad} = 0.49 \pm 0.04$ J/m^2; Au (100)–sapphire (0001): 2.18 ± 0.06 J/m^2, $W_{ad} = 0.55 \pm 0.07$ J/m^2.

Introduction

Solid–liquid interfaces

High temperature wetting experiments are often used to extract interfacial thermodynamic data, such as the thermodynamic work of adhesion (W_{ad}) and interfacial energies, for solid–liquid systems. In its simplest form, the relative surface energies of the solid-liquid system are represented by the contact angle (θ), which is often used as a comparative measure of wetting for processes such as soldering, brazing, and liquid phase sintering [1] (see Fig. 1). More detailed analysis provides values of the various surface energies of the system, which together with careful characterization can provide a means to correlate interfacial energies with Gibbsian segregation [2–6].

The most common method to measure wetting is the sessile drop experiment, which is based on a liquid drop equilibrated in contact with a solid substrate. When thermodynamic equilibrium is achieved, and provided that the interface remains flat and co-planar with the substrate [7], the contact angle (θ) can be used via Young's equation as a measure of the substrate-vapor (γ_{SV}), liquid–vapor (γ_{LV}), and substrate–liquid (γ_{SL}) interfacial energies [1]:

$$\gamma_{SV} = \gamma_{SL} + \gamma_{LV}\cos\theta \tag{1}$$

The thermodynamic work of adhesion (W_{ad}) is defined as the energy gained (or expended) to form an equilibrated interface from two equilibrated free surfaces [2, 7, 8], and can be expressed via the Dupré equation:

$$W_{ad} = \gamma_{LV} + \gamma_{SV} - \gamma_{SL} \tag{2}$$

If the surface energy of the liquid is known or measured, W_{ad} can be determined from the contact angle via the Young–Dupré equation:

$$W_{ad} = \gamma_{LV}(1 + \cos\theta) \tag{3}$$

H. Sadan · W. D. Kaplan (✉)
Department of Materials Engineering, Technion – Israel Institute of Technology, Haifa 32000, Israel
e-mail: kaplan@tx.technion.ac.il

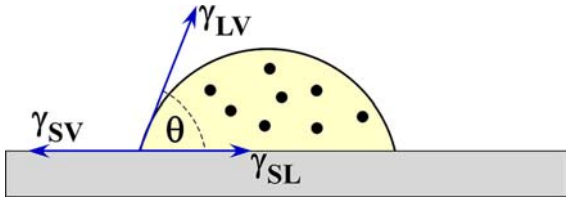

Fig. 1 Schematic drawing of a sessile drop on a flat solid substrate. The solid–liquid interface is co-planar with the substrate surface

Solid–solid interfaces

The measurement of solid–solid interface energies is equally important, although more difficult to access. The thermodynamic work of adhesion of solid-solid interfaces is significant for the evaluation of mechanical properties, such as the strength of joins and fracture energy [9–11]. For example, using a gold-sapphire model system Lipkin et al. found that a reduction of ~40% in the work of adhesion, associated with preferred segregation of carbon to the free surfaces, results in a decrease in the fracture energy by two orders of magnitude [11]. While it is clear that the fracture energy of a solid–solid interface depends on the interface energy, this correlation is not necessarily linear and will depend on interfacial segregation as well as dissipative processes (i.e. plastic deformation). As such, fundamental analysis of the properties of solid–solid interfaces requires a rigorous method for the measurement of interfacial energies.

The analysis of solid surfaces and interfaces requires a different approach than that of liquids, since solid surface and interface energies can be anisotropic. Due to anisotropy, a solid particle can have a facetted rather than a round equilibrium shape. The equilibrium shape is known as the Wulff shape [12], and is achieved by the minimization of total surface energy via optimization of relative surface areas of different crystallographic planes, for a given particle volume. The relative surface energy of these planes can be determined by analyzing the geometry of the particle [13–15].

One of the most commonly used theories for the measurement of solid–solid interfacial energy was developed by Winterbottom [16]. This approach is based on geometrical analysis of the Wulff shape of a single crystal equilibrated on a solid substrate of a dissimilar material. The interfacial energy can be determined by measuring two characteristic lengths: the distance from the center of the Wulff plot (i.e. the Wulff point) to the interface with the substrate (R_1), and the distance from the Wulff point to the uppermost facet of the particle (R_2), as shown schematically in Fig. 2.

By measuring R_1 and R_2, the interfacial energy can be determined using:

$$\frac{R_1}{R_2} = \frac{\gamma_{sp} - \gamma_{sv}}{\gamma_{pv}} \tag{4}$$

where γ_{SP} is the substrate–particle interfacial energy, γ_{SV} is the surface energy of the substrate, and γ_{PV} is the surface energy of the uppermost particle facet [16, 17]. It should be noted that this approach only applies to single-crystal particles, and a flat interface which is co-planar with the substrate surface [18]. In order to determine the interface energy, the orientation of both the particle and the substrate must be known. In addition, for an accurate determination of the Wulff point (and consequently R_1 and R_2), a full 3-dimensional analysis of the particle shape is necessary.

The goal of this work is to develop an experimental methodology for the measurement of solid–solid interfacial energies, and to apply it to the Au-(0001) sapphire interface.

Experimental methods

Dewetting experiments

Basal plane (0001)-oriented sapphire (α-Al_2O_3) substrates of 99.99% purity were provided by Gavish Industrial Technologies & Materials. Substrates were ultrasonically cleaned in acetone and ethanol, and

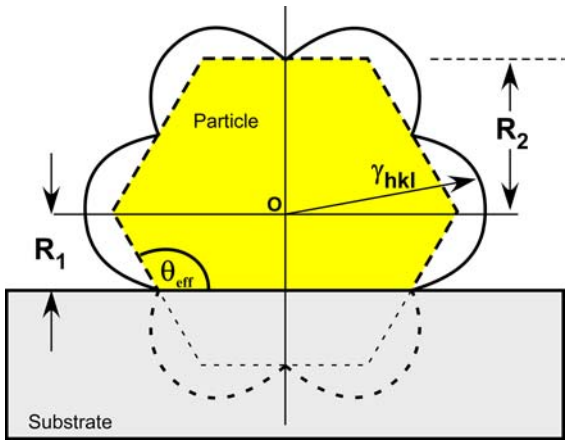

Fig. 2 Schematic drawing of the Winterbottom analysis for a particle equilibrated on a substrate, having an effective contact angle $\theta > 90$ °. The black curve indicates the γ-plot of an isolated particle. The dashed polyhedron indicates the resulting equilibrium Wulff shape and its center O (the Wulff point). R_1 and R_2 are the distances from the Wulff point to the interface with the substrate and to the uppermost particle facet, respectively

thermally annealed for 2 h at 1200 °C in air. A ~20 nm thick Au film was deposited on the substrates using a Polaron sputter coater. The specimens were annealed in air at 1100 °C for 30 min. Since at this temperature Au is in a liquid state (T_m = 1064 °C), dewetting of the film will occur due to the finite contact angle of Au with sapphire. This resulted in an extremely large number of sub-micron droplets. Specimens were then cooled to 1000 °C ($0.95T_m$) and annealed for various durations of time (0.5, 5, 10, 20, 50 and 100 h) in order to reach equilibrium. This process resulted in faceted particles with diameters varying from 100 nm to 900 nm (see Fig. 3).

The morphology of the equilibrated particles was compared to that of particles which were cooled from 1100 °C to room temperature, at the same rate. It was found that the particles which were cooled without equilibration at 1000 °C were, for the most part, round in shape. In addition, as will be shown below, the particles equilibrated at 1000 °C had similar facet morphologies. This led to the conclusion that the Au particles were in the solid state during equilibration.

Characterization methods

The morphology and relative orientation of the equilibrated Au particles were examined by high resolution scanning electron microscopy (HRSEM) and electron backscattered diffraction (EBSD). HRSEM was conducted on a LEO 982 Gemini microscope equipped with a field emission gun (FEG–SEM). Top-view secondary electron images were recorded using an accelerating voltage of 5 kV, and a working distance of 3–5 mm. EBSD patterns were acquired and indexed using a Link Opal EBSD System (Oxford Instruments, UK) [19], consisting of a low intensity electron sensitive unit mounted on the HRSEM and connected to a computer. EBSD measurements were conducted at 20 kV with a ~3 nA electron-probe current, at a 20 mm working distance. The distance between the interaction region in the sample and the CCD camera was 40 mm. The angle between the sapphire substrate normal and the electron probe was 70°. The standard sample used for EBSD pattern calibration was (001) Si. The integration time used for EBSD pattern and background acquisition was 1.3 sec.

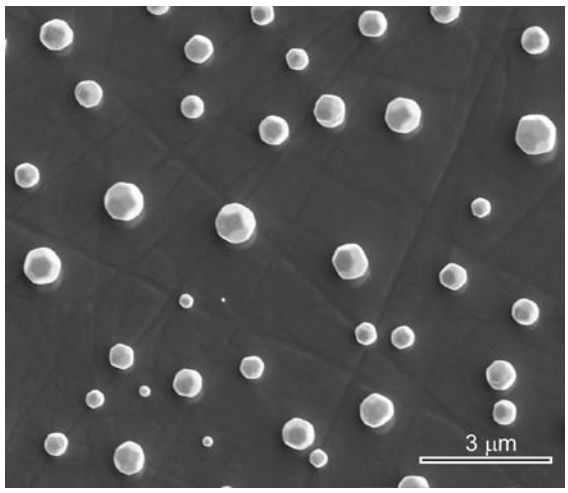

Fig. 3 Secondary electron SEM micrograph of Au particles equilibrated on a (0001) sapphire substrate at 1000 °C for 100 h

The Au particle orientation distribution was also examined by X-ray diffraction (XRD), using a conventional X-ray diffractometer (Philips X'Pert goniometer) with CuKα radiation operated at 40 mA and 40 kV. A θ–2θ coupled Bragg-Brentano geometry was used for subsequent analysis of integrated intensities and the preferred orientation of Au reflections relative to the sapphire substrate. 2θ scans were acquired from 35 ° to 140 ° with a step size of 0.04 ° and an exposure time of 15 sec per step.

High resolution transmission electron microscopy (HRTEM) was conducted on a JEOL 3010 UHR microscope, operated at 300 kV and with a point resolution better than 0.16 nm. HRTEM was used to determine the interface plane and orientation relationship between the particles and the sapphire substrate using Kikuchi and selected area electron diffraction (SAD).

A dual beam FIB (FEI Strata 400 STEM) equipped with a high angle annular dark field (HAADF) scanning transmission electron microscopy (STEM) detector and nano-manipulator (Omniprobe, AutoProbe 200) was used for several applications, including:

- Cross-sectioning of the Au particles to determine whether they contain grain boundaries, and for examination of the Au-sapphire interface;
- Preparing TEM specimens from the center of particles with a known morphology and orientation using the ''lift out'' technique [20, 21];
- Performing serial-sectioning through the particles, with high resolution (electron) imaging following the creation of each slice [22]. The acquired images were used for 3-dimensional reconstruction using the ''Reconstruct'' software package [23]. The serial-sectioning procedure is schematically illustrated in Fig. 4. The FIB was also used for milling a triangular depression adjacent to the sliced particle. This shape of known dimensions (characterized using the SEM mode of the FIB) was also included in the serial-sectioning procedure, and was used as a two dimensional scale bar for internal calibration of the slice thickness.

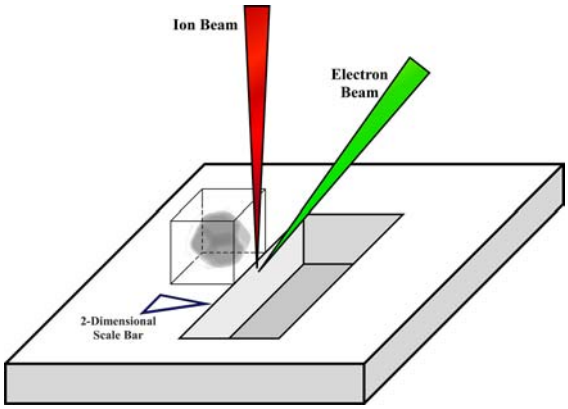

Fig. 4 Schematic drawing of the FIB serial-sectioning procedure. A protective Pt coating was first deposited on the particle, using the electron beam, in order to prevent damage to the surface of the particle by the ion beam. A box was milled in front of the coated particle which allowed for subsequent electron beam imaging of the interface. The triangular-shaped 2-dimensional scale bar was etched by FIB prior to serial-sectioning, and was used to calibrate the thickness of each slice

Results

Determination of preferred orientation

An equilibrium orientation relationship of a particle with the substrate indicates a possible low-energy configuration, analogous to cusps in plots of grain boundary energy versus misorientation [14, 24, 25]. While electron diffraction in TEM is the preferred method to characterize an orientation relationship, the lack of statistics available from reasonable TEM studies is less than satisfactory. As a first step in the analysis of the particle orientation, EBSD patterns were acquired from 20 different particles from each sample (equilibrated at different times at 1000 °C), and the results are presented in Fig. 5. The results did not show any detectable preferred orientation of Au on the sapphire substrate, and from these results alone the time required to reach equilibrium could not be determined.

In a separate series of experiments, a stable preferred orientation of Au particles on the prismatic $(10\bar{1}0)$ plane of sapphire, dewetted under identical conditions, was achieved after no more than 5 h. These results, which will be published elsewhere, lead to the conclusion that equilibrium of Au particles on the basal surface of sapphire is reached after the same time, and the fact that no preferred orientation was detected by EBSD on the basal surface of sapphire, even after much longer annealing times, is probably not because more time is required to reach equilibrium.

A possible explanation for the fact that no preferred orientation was detected by EBSD is that this method only provides information from ~40 nm below the surface [19]. If a Au particle contains a grain boundary, it is not possible to determine the orientation of the particle (grain) adjacent to the sapphire. It should be noted that visual (HRSEM) inspection of the particles to determine if grain boundaries were present could not be conducted during EBSD measurements, since at these working conditions (20 kV) the resolution of the HRSEM is limited.

Unlike EBSD, the results from XRD did indicate the presence of two possible preferred orientations of the Au particles: Au (111) ‖ sapphire (0001) and Au (100) ‖ sapphire (0001) (see Table 1). These two contradicting sets of results imply the possibility of a different Au particle orientation adjacent to the substrate compared to the top surface of the particle, i.e., some of the particles are not single crystals.

Particle morphology

Morphological examination of the particles equilibrated for 100 h was conducted using HRSEM. The results confirmed that many of the particles (73%) contained grain boundaries, as shown in Fig. 6. From the symmetry of the surface facets relative to the orientation of the grain boundaries, many of the grain boundaries were identified as twin boundaries. In addition, general high angle and low angle grain boundaries were also identified, similar to comparable experiments conducted on Cu particles [26].

Among the particles that did not contain any detectable grain boundary grooves, only three different

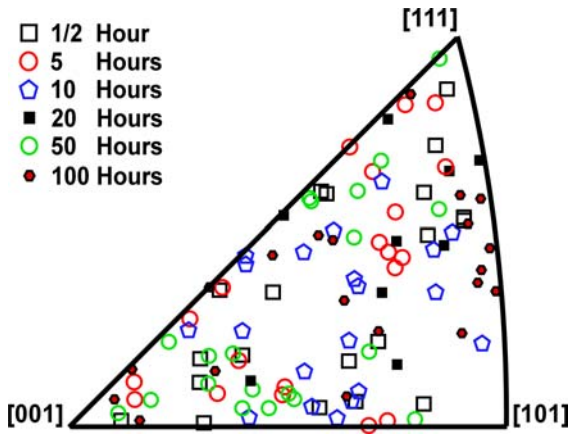

Fig. 5 Inverse pole figure from Au particles, dewetted on the basal sapphire surface at 1000 °C as a function of time (data from EBSD-SEM). 20 particles were characterized for each annealing time, except for the sample equilibrated for 20 h, for which nine particles were characterized

Table 1 Integrated XRD intensities for Au particles equilibrated on (0001) sapphire for 100 h (sapphire reflections excluded). Simulated intensities were generated from a computer program (Rietica 1.7.7) and took into account the thin film nature of the particles

Reflection	2θ	Measured intensity (I)	Simulated intensity (I')	$P_{hkl} = \frac{I(hkl)}{I'(hkl)} \cdot \frac{\sum I'(hkl)}{\sum I(hkl)}$
(111)	38.203	100	100	1.54
(200)	44.403	48.8	48.7	1.55
(220)	64.604	12.9	31.0	0.64
(311)	77.602	7.0	36.0	0.30
(331)	110.882	0.9	19.2	0.08
(420)	115.330	1.2	19.2	0.09
(422)	135.512	1.2	22.9	0.08

P indicates a measure of preferred orientation. A value of P equal to one indicates a random distribution of planes. P greater than one indicates a preferred orientation. Summation was conducted over all the listed Au reflections

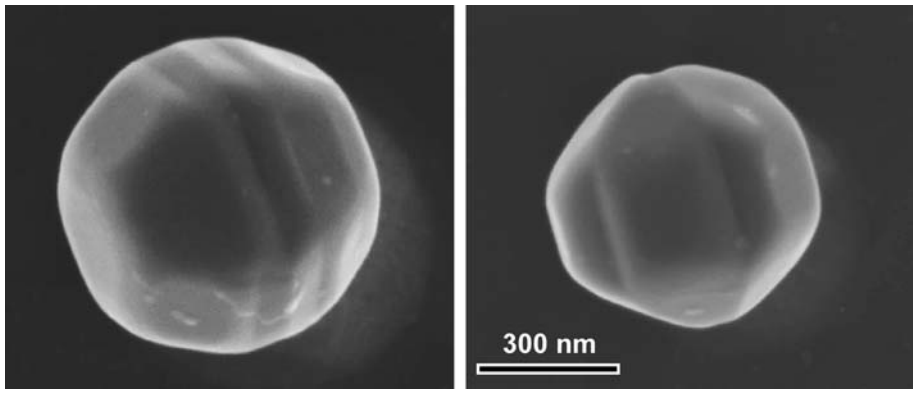

Fig. 6 Secondary electron SEM micrographs of Au particles containing visible grain boundary grooves. The scale bar is equivalent for both micrographs

repeating morphologies were observed. These equilibrium shapes and their frequency of appearance are presented in Fig. 7, and Table 2, respectively.

Morphological examination revealed that the particles were highly faceted, unlike reports from other works [27, 28]. The difference in the relative surface area of the facets may be due to the fact that the particles in this experiment were equilibrated in air, and not in vacuum [27, 28]. In addition, and/or as a result, it is possible that impurity elements have segregated to the surface of the Au, decreasing the surface energies of the facet planes. While it is normally accepted that segregation occurs to high energy surfaces in order to lower their surface energy, thus reducing the surface anisotropy, exceptions have been found where segregation to low energy surfaces is preferred, for example Pb doped with Ni and Bi [29], and Cu doped with Bi [30].

Interfacial energy measurements

The most common particle morphology which did not contain grain boundaries is shown in Fig. 7(c) (see Table 2). This equilibrium shape and interface orientation probably relates to a minimum in the total surface (free surface and interface) energy [31].

Three dimensional reconstruction using FIB serial-sectioning was conducted for two other particles with the same morphology and orientation with the substrate as the particles shown in Fig. 7(b, c). The thickness of each slice was set to be 10 nm. However, the actual slice thickness determined using the

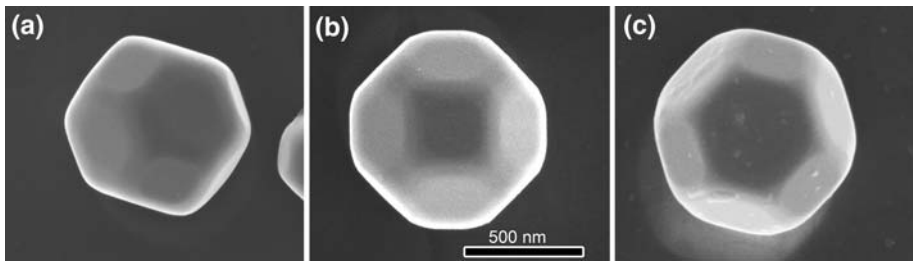

Fig. 7 Secondary electron SEM micrographs showing the three (**a**–**c**) typical morphologies of the Au particles which did not contain grain boundaries

Table 2 Frequency of appearance of the different particle morphologies. The statistics are based on HRSEM examination of 210 particles

Particle morphology	Figure 7(a)	Figure 7(b)	Figure 7(c)	Particles containing grain boundaries
Frequency of appearance	10.3%	3.6%	12.9%	73.2%

2-dimensional scale bar varied in the range of 12–13 nm. R_1 and R_2 were measured from the reconstructed particles and individual slices (Fig. 8). The estimated error of the ratio R_1/R_2, as measured from the reconstructed particle and from individual slices, is ~15%.

TEM specimens were prepared using the dual-beam FIB from the center of particles with the morphologies shown in Fig. 7(b, c). The orientation relationship of the particle seen in Fig. 7 (c) was determined to be: Au (111) || sapphire (0006), Au [$2\bar{2}0$] || sapphire [$2\bar{1}\bar{1}0$] (see Fig. 9).

Once the orientation relationship was determined, the interfacial energy was calculated using Eq. (4). Surface energies were taken from the literature; 1.4 J/m^2 for Au (111) [32, 33], and 1.24 J/m^2 for (0001) sapphire [34]. Using R_1 and R_2 measured from the TEM micrograph, the Au (111)-sapphire (0001) interfacial energy was determined to be $\gamma_{SP} = 2.15 \pm 0.04$ J/m^2, resulting in $W_{ad} = 0.49 \pm 0.04$ J/m^2. This value is relatively low, as should be expected, since the adhesion between Au and sapphire is quite poor.

The orientation relationship of the particle seen in Fig. 7(b) was determined from TEM analysis to be: Au (002) || sapphire (0006), Au [$2\bar{2}0$] || sapphire [$1\bar{2}10$] (see Fig. 10). The cross-sections made in the particle with the Au (100) plane parallel to the interface with the substrate show an inclination of the particle of ~2° with respect to the substrate. This can be clearly seen in Fig. 8 (b) and Fig. 10. The deviation from a low-index orientation relationship was measured from the diffraction pattern to be ~2.2°. Higher magnification TEM analysis of the interface acquired off zone-axis revealed a periodic array of dislocations at the interface. These dislocations probably serve to reduce strain energy at the interface, and are the likely reason for inclination of the particle.

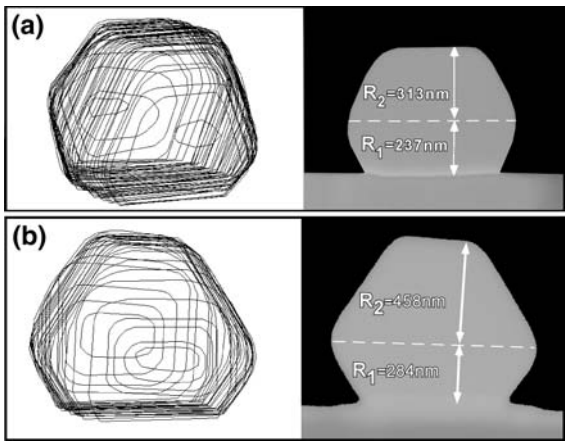

Fig. 8 Three-dimensional reconstruction of a Au particle from FIB serial-sectioning, and a single slice from the center of the particle from which R_1 and R_2 were measured. (**a**) is from a particle having the same morphology as Fig. 7(c), and (**b**) is from a particle having the same morphology as Fig. 7(b)

In addition to R_1, R_2 and γ_{sv}, the Au (200) surface energy was required to determine the interfacial energy for the particle shown in Fig. 10. Instead of using surface energies from the literature, which were derived from particles equilibrated under different experimental conditions than those used here, the equilibrium shape of the particle in Fig. 9 was used to determine the surface energy of the (100) facet. Starting with a value of 1.4 J/m^2 for γ(111) [32, 33], the ratio of the normals from the Wulff point to the (111) and (100) facets was used to calculate γ(100). It was found that the surface energy of Au (100) is 1.49 ± 0.04 J/m^2. Using this value, it was found that the Au (100)-sapphire (0001) interfacial energy is 2.18 ± 0.06 J/m^2, and W_{ad} is 0.55 ± 0.07 J/m^2.

A comparison of the values of the two interfacial energies indicates that the difference is within the error range. This implies that these two preferred orientations should appear with a similar frequency, as was confirmed from the XRD. However, the frequency of particles detected by SEM having the morphology shown in Fig. 7(b) is lower than that of the particles shown in Fig.7(c). This is probably due to the difference in the total surface energy (free surfaces and interface) of the system.

Discussion

The preferred orientation and possible orientation relationships of Au on (0001) sapphire was investigated previously by Fecht and Gleiter, using pole figures determined from XRD [35], resulting in a preferred orientation similar to the results presented here.

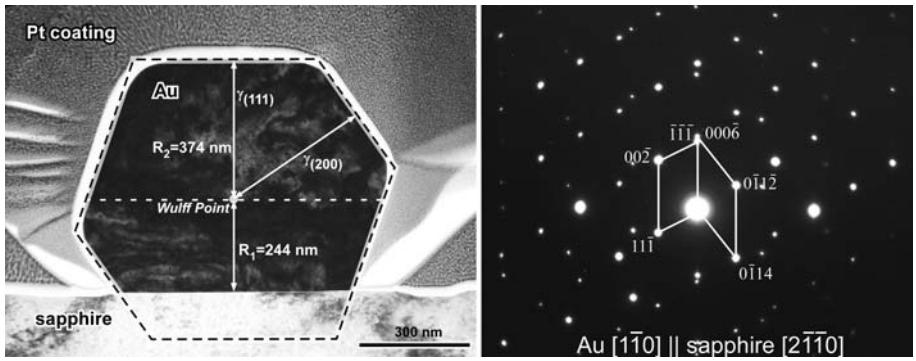

Fig. 9 Bright field TEM micrograph and SAD patterns of a Au particle and the sapphire substrate. The sample was prepared from a particle with the morphology shown in Fig. 7(c). Kikuchi electron diffraction was used to orient the substrate in the [2$\bar{1}\bar{1}$0] zone-axis, before acquiring the SAD patterns

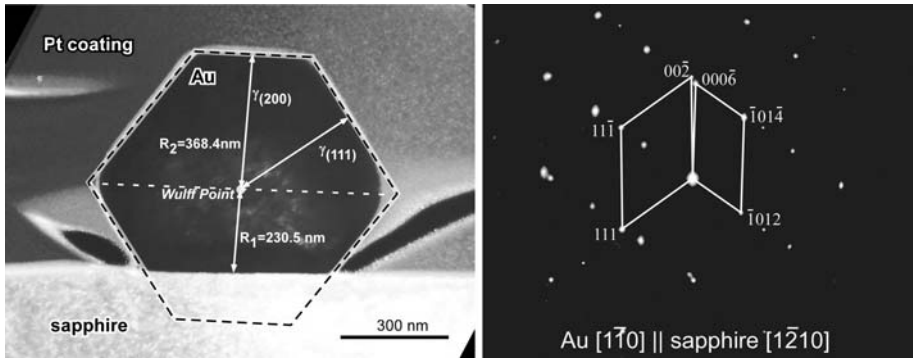

Fig. 10 Dark field TEM micrograph and selected area diffraction patterns for a Au particle and the sapphire substrate. The sample was prepared from a particle with the morphology shown in Fig. 7(b). Kikuchi electron diffraction was used to orient the substrate in the [1$\bar{2}$10] zone-axis, before acquiring the SAD patterns

However, Fecht and Gleiter found that the Au (111) || sapphire (0001) orientation had a higher frequency of appearance than Au (100) || sapphire (0001), indicating a lower surface and interface energy configuration of the system. Our morphological analysis shows a statistically higher appearance of Au (111) || sapphire (0001), which agrees with the results of Fecht and Gleiter. However, the morphological analysis was only conducted on single crystal particles, which did not contain any visible grain boundaries, as opposed to the XRD results presented here, which sampled all of the particles. Furthermore, our analysis of the relative interfacial energies does not indicate an appreciable interfacial energy difference between these two orientation relationships, as was corroborated by XRD.

The fact that the facet area is relatively large, is attributed to preferred segregation of impurities to the facet planes, and hence an increase in the surface anisotropy. Mullins et al. [36] and Rohrer et al. [37] have shown that in order for a facet to reach its full equilibrium size, a nucleation barrier for facet growth and shrinkage needs to be overcome. As a result, facets larger than a critical size (i.e. a few nanometers) will not reach their equilibrium size, unless some step-generating defects are present, such as screw dislocations emerging from the facet plane. This results in a difference in the surface anisotropy for different particle sizes, which is dependent on the density of dislocations, and can lead to inaccuracy in the relative surface energy measurement [26]. However, the Au particles examined in the present study had relatively large facet size, and no inhibition in facet growth or shrinkage was apparent. In addition, no significant change in the surface anisotropy was detected for different particle sizes (although only qualitative measurements of the anisotropy were conducted). This leads to the conclusion that no kinetic inhibition on the facet size occurred in the examined system, i.e. the shape of the Au particles is indeed the equilibrium shape for the experimental conditions used here [30].

The estimated errors in the measurement of R_1/R_2 using FIB serial sectioning are ~15%, and only ~4% using TEM. Although use of reconstructed particles results in better statistics and enables measurements from multidirectional cross-sections, the use of the TEM provides better resolution and hence more accurate measurements, in addition to the ability to determine the orientation of the particle with the substrate, and the presence of steps or dislocations at the interface.

The values for the interfacial energy and W_{ad} determined in the present work do not agree with the values determined by Pilliar and Nutting [17] (see Table 3 for a comparison). It should be noted that their analysis was also based on Winterbottom's approach. However, they used *polycrystalline* alumina substrates

Table 3 Interfacial energy and W_{ad} of Au–Al_2O_3 interfaces in air. The values were determined using the surface energies: Au (111) = 1.4 J/m^2, and 1.24 J/m^2 for (0001) sapphire. The values in parenthesis are the original values in the cited references which were determined using various values for the surface energy of alumina and gold

	Interface Energy [J/m^2]	W_{ad} [J/m^2]	Reference	Temperature [°C]
Au–alumina	2.52 (1.725)	0.12 (0.53)	[17]	1000
Au–sapphire (0001)	2.08 (1.74)	0.56 (0.6)	[11]	1030 – 1050
Au (111)–sapphire (0001)	2.15 ± 0.04	0.49 ± 0.04	This work	1000
Au (100)–sapphire (0001)	2.18 ± 0.06	0.55 ± 0.07	This work	1000

rather than sapphire. As a result, the interfacial energy that Pilliar and Nutting determined was an average value for all of the substrate crystal orientations. Furthermore, the shape of the particles was determined using a shadowing technique from thick TEM specimens, making determination of the Wulff point extremely difficult, which limits the accuracy in determining R_1 and R_2. Pilliar and Nutting evaluated the inaccuracy of their results to be no more than 20%. Although *all* of the particles they found on alumina grains with a (0001) facet were identified as having the Au (111) plane parallel to the substrate, no variation of the interfacial energy was found, even when the interface energy was compared to that of Au in contact with $(5\bar{5}02)$ Al_2O_3.

While Lipkin et al. determined the interfacial energy and W_{ad} from contact angle measurements of voids at the interface between solid gold films and sapphire, rather than from Winterbottom's approach [11], the results show very good agreement with the values determined in this work. A rigid interpretation of solid-solid interfacial energies from contact angles requires analysis of torque terms [38, 39]. Using Winterbottom's approach the torque terms are included in the analysis, as long as the interface is flat and co-planar with the substrate [18]. Regardless of this, the results from Lipkin *et al.* and the results from this study agree.

To the authors' best knowledge, no previous work was conducted on the morphology of Au particles equilibrated on sapphire substrates. Au particles equilibrated on α-SiC under UHV at 580 °C [27, 28, 40] were studied by Wynblatt and co-workers, including compositional analysis by Auger spectroscopy, which showed no detectable level of impurities. Given that no segregation from the substrate or environment occurred, the Au particles studied by Wynblatt and co-workers have the morphology of pure Au crystals. As was already discussed, the particles investigated in this work were highly faceted, and contained fewer rough surfaces than the pure Au particles on α-SiC. This may be due to impurity segregation (adsorption) from the air atmosphere used in this study [3, 6, 11, 27]. In both cases, deeper cusps in the Au γ-plot associated with (111) and (100) planes results in faceted surfaces. The fact that a large portion of the examined particles contained grain boundaries may imply that grain boundary segregation occurred resulting in a decrease in Au grain boundary energy [27, 28]. In addition, if segregation occurred, the value of the γ-Au (111) surface energy is probably lower than the one applied in Eq. (4) [32, 33]. The lack of a methodology for the calculation or measurement of absolute surface energies of segregated surfaces poses a major problem in determining interfacial energies, using both contact angle measurements and Winterbottom's analysis. Since the spatial resolution of surface analysis techniques, such as Auger, are greater than the Au particle size (due to backscattered electrons), analytical TEM is required to correlate surface (and interface) chemistry with changes in surface energy. This will be the focus of a future study.

The use of Winterbottom's approach is not preferred over dihedral angle measurements, for the case of an effective contact angle smaller than 90°, where less than half of the Wulff shape is visible. In this case, the position of the Wulff point can be determined only by correlating the equilibrium shape with the shape of the same particle in another system [41], providing no segregation has occurred and the surface energy ratio has not changed.

Summary and conclusions

The purpose of this work was to develop a methodology to determine solid-solid interfacial energy. Samples were made by dewetting thin gold films on a sapphire substrates. This resulted in an extremely large number of submicron-sized particles, which were equilibrated at 1000 °C. In order to use Winterbottom's analysis, the aspect ratio of an equilibrated particle was determined using two different methods: FIB serial-sectioning and TEM, from which the latter was found to be more accurate. Impurity segregation is believed to have decreased the grain boundary energy

and surface energy of the (111) and (100) gold facets, resulting in larger facet areas and a relatively low percentage of single crystals. The presence of two preferred orientations was determined using XRD, and the absolute interfacial energy as well as the thermodynamic work of adhesion were determined: Au (111)-sapphire (0001): $\gamma_{SP} = 2.15 \pm 0.04$ J/m^2, $W_{ad} = 0.49 \pm 0.04$ J/m^2. Au (100)-sapphire (0001): 2.18 ± 0.06 J/m^2, W_{ad} is 0.55 ± 0.07 J/m^2.

Acknowledgements The authors thank D. Chatain, P. Wynblatt, and D. Brandon for enlightening discussions. The thought-provoking comments of the anonymous referee were very much appreciated. This research was partially supported by the Israel Science Foundation ((163/05) and the Russell Berrie Nanotechnology Institute at the Technion.

References

1. Young T (1805) Philos Trans R Soc 65:95
2. Humenik M Jr., Kingery WD (1954) J Am Ceram Soc 37:18
3. Wynblatt P (2000) Acta Materialia 48:4439
4. Monchoux JP, Chatain D, Wynblatt P (2004) Appl Surf Sci 228:357
5. Shim H, Wynblatt P, Chatain D (2000) Surf Sci 465:97
6. Rao GZ, Wynblatt DBP (1993) Acta Metallurgica et Materialia 41:3331
7. Murr LE (1973) Mater Sci Engineer 12:277
8. Eustathopoulos N, Nicholas MG, Drevet B (1999) In: Wettability at high temperatures. Pergamon Materials Series v.3, Oxford, UK, p 43
9. Lipkin DM, Israelachvili JN, Clarke DR (1997) Philos Mag A 76:715
10. Dalgleish BJ, Saiz E, Tomsia AP, Cannon RM, Ritchie RO (1994) Scripta Metallurgica Et Materialia 31:1109
11. Lipkin DM, Clarke DR, Evans AG (1998) Acta Materialia 46:4835
12. Wulff G, Krystallogr Z (1901) Mineral 34:449
13. Herring C (1954) Phys Rev 82:87
14. Blendell JE, Carter WC, Handwerker CA (1999) J Am Ceram Soc 82:1889
15. Heyraud JC, Metois JJ (1980) J Crystal Growth 50:571
16. Winterbottom WL (1967) Acta Metallurgica 15:303
17. Pilliar RM, Nutting J (1967) Philos Mag 16:181
18. Cahn JW, Hoffman DW (1974) Acta Metallurgica 22:1205
19. Dingley D (2004) J Microsc 213:214
20. Sivel VGM, Van Den Brand J, Wang WR, Mohdadi H, Tichelaar FD, Alkemade PFA, Zandbergen HW (2004) J Microsc 214:237
21. Reyntjens S, Puers R (2001) J Micromech Microeng 11:287
22. Holzer L, Indutnyi F, Gasser PH, Munch B, Wegmann M (2004) J Microsc 216:84
23. Fiala JC (2004) J Microsc 218:52
24. Heremann G, Gleiter H, Baro G (1975) Acta Metallurgica 24:353
25. Saylor DM, Rohrer GS (1999) Proceedings of the international conference on textures of materials, 12th, Montreal QC, Canada, Aug. 9–13, 1999 2 (1999) 1690
26. Chatain D, Ghetta V, Wynblatt P (2004) Interface Sci 12:7
27. Wang Z, Wynblatt P (1998) Acta Materialia 46:4853
28. Wang Z, Wynblatt P (1998) Surf Sci 398:259
29. Cheng WC, Wynblatt P (1997) J Crystal Growth 173:513
30. Chatain D, Wynblatt P, Rohrer GS (2005) Acta Materialia 53:4057
31. Siem EJ, Carter WC, Chatain D (2004) Philos Mag 84:991
32. Bonzel HP, Nowicki M (2004) Phys Rev B 70:245430
33. Leadbeater CJ (1951) Powder Metall 9:1
34. Levi G, Kaplan WD (2003) Acta Materialia 51:2793
35. Fecht HJ, Gleiter H (1985) Acta Metallurgica 33:557
36. Mullins WW, Rohrer GS (2000) J Am Ceram Soc 83:214
37. Rohrer GS, Rohrer CL, Mullins WW (2001) J Am Ceram Soc 84:2099
38. Herring C (1951) In: Kingston WE (ed) The physics of powder metallurgy, McGraw-Hill, New York, p 143
39. Hodgson BK, Mykura H (1973) J Mater Sci 8:565
40. Emundts A, Bonzel HP, Wynblatt P, Thurmer K, Reutt-Robey J, Williams ED (2001) Surf Sci 481:13
41. Hansen KH, Worren T, Stempel S, Laegsgaard E, Baumer M, Freund HJ, Besenbacher F, Stensgaard I (1999) Phys Rev Lett 83:4120